



This is a repository copy of *JWST/NIRSpec observations of the coldest known brown dwarf\**.

White Rose Research Online URL for this paper:

<https://eprints.whiterose.ac.uk/206433/>

Version: Published Version

---

**Article:**

Luhman, K.L. [orcid.org/0000-0003-2822-2951](https://orcid.org/0000-0003-2822-2951), Tremblin, P. [orcid.org/0000-0001-6172-3403](https://orcid.org/0000-0001-6172-3403), Alves de Oliveira, C. [orcid.org/0000-0003-2896-4138](https://orcid.org/0000-0003-2896-4138) et al. (6 more authors) (2024) *JWST/NIRSpec observations of the coldest known brown dwarf\**. *The Astronomical Journal*, 167 (1). 5. ISSN 0004-6256

<https://doi.org/10.3847/1538-3881/ad0b72>

---

**Reuse**

This article is distributed under the terms of the Creative Commons Attribution (CC BY) licence. This licence allows you to distribute, remix, tweak, and build upon the work, even commercially, as long as you credit the authors for the original work. More information and the full terms of the licence here:

<https://creativecommons.org/licenses/>

**Takedown**

If you consider content in White Rose Research Online to be in breach of UK law, please notify us by emailing [eprints@whiterose.ac.uk](mailto:eprints@whiterose.ac.uk) including the URL of the record and the reason for the withdrawal request.



[eprints@whiterose.ac.uk](mailto:eprints@whiterose.ac.uk)  
<https://eprints.whiterose.ac.uk/>



# JWST/NIRSpec Observations of the Coldest Known Brown Dwarf\*

K. L. Luhman<sup>1,2</sup> , P. Tremblin<sup>3</sup> , C. Alves de Oliveira<sup>4</sup> , S. M. Birkmann<sup>5</sup> , I. Baraffe<sup>6,7</sup> , G. Chabrier<sup>6,7</sup> ,  
E. Manjavacas<sup>8,9</sup> , R. J. Parker<sup>10,12</sup> , and J. Valenti<sup>11</sup>

<sup>1</sup> Department of Astronomy and Astrophysics, The Pennsylvania State University, University Park, PA 16802, USA; [kil207@psu.edu](mailto:kil207@psu.edu)

<sup>2</sup> Center for Exoplanets and Habitable Worlds, The Pennsylvania State University, University Park, PA 16802, USA

<sup>3</sup> Université Paris-Saclay, UVSQ, CNRS, CEA, Maison de la Simulation, F-91191 Gif-sur-Yvette, France

<sup>4</sup> European Space Agency, European Space Astronomy Centre, Camino Bajo del Castillo s/n, E-28692 Villanueva de la Cañada, Madrid, Spain

<sup>5</sup> European Space Agency (ESA), ESA Office, Space Telescope Science Institute, 3700 San Martin Drive, Baltimore, MD 21218, USA

<sup>6</sup> Physics & Astronomy Dpt, University of Exeter, Exeter EX4 4QL, UK

<sup>7</sup> Ecole Normale Supérieure de Lyon, CRAL, CNRS UMR 5574, F-69364 Lyon Cedex 07, France

<sup>8</sup> AURA for the European Space Agency, Space Telescope Science Institute, 3700 San Martin Drive, Baltimore, MD 21218, USA

<sup>9</sup> Department of Physics & Astronomy, Johns Hopkins University, Baltimore, MD 21218, USA

<sup>10</sup> Department of Physics and Astronomy, The University of Sheffield, Hicks Building, Hounsfield Road, Sheffield S3 7RH, UK

<sup>11</sup> Space Telescope Science Institute, 3700 San Martin Drive, Baltimore, MD 21218, USA

Received 2023 September 30; revised 2023 November 7; accepted 2023 November 8; published 2023 December 5

## Abstract

We present 1–5  $\mu\text{m}$  spectroscopy of the coldest known brown dwarf, WISE J085510.83–071442.5 (WISE 0855), performed with the Near-Infrared Spectrograph (NIRSpec) on board the James Webb Space Telescope (JWST). NIRSpec has dramatically improved the measurement of the spectral energy distribution (SED) of WISE 0855 in terms of wavelength coverage, signal-to-noise ratios, and spectral resolution. We have performed preliminary modeling of the NIRSpec data using the ATMO 2020 models of cloudless atmospheres, arriving at a best-fitting model that has  $T_{\text{eff}} = 285$  K. That temperature is  $\sim 20$  K higher than the value derived by combining our luminosity estimate with evolutionary models (i.e., the radius in the model fit to the SED is somewhat smaller than expected from evolutionary models). Through comparisons to the model spectra, we detect absorption in the fundamental band of CO, which is consistent with an earlier detection in a ground-based spectrum and indicates the presence of vertical mixing. Although  $\text{PH}_3$  is expected in Y dwarfs that experience vertical mixing, it is not detected in WISE 0855. Previous ground-based  $M$ -band spectroscopy of WISE 0855 has been cited for evidence of  $\text{H}_2\text{O}$  ice clouds, but we find that the NIRSpec data in that wavelength range are matched well by our cloudless model. Thus, clear evidence of  $\text{H}_2\text{O}$  ice clouds in WISE 0855 has not been identified yet, but it may still be present in the NIRSpec data. The physical properties of WISE 0855, including the presence of  $\text{H}_2\text{O}$  clouds, can be better constrained by more detailed fitting with both cloudless and cloudy models and the incorporation of unpublished 5–28  $\mu\text{m}$  data from the Mid-infrared Instrument on JWST.

*Unified Astronomy Thesaurus concepts:* [Brown dwarfs \(185\)](#); [Y dwarfs \(1827\)](#); [Exoplanet atmospheres \(487\)](#)

*Supporting material:* data behind figures

## 1. Introduction

Y is the coldest spectral class of brown dwarfs ( $T_{\text{eff}} \lesssim 500$  K; Cushing et al. 2011; Kirkpatrick et al. 2021). Because the near-infrared (NIR) fluxes of brown dwarfs collapse from late T into the Y class (Kirkpatrick et al. 2011), sensitive space-based telescopes operating at mid-infrared (MIR) wavelengths offer the best opportunity for detecting Y dwarfs. Given their extremely low luminosities, detections of Y dwarfs are restricted to the solar neighborhood, whose members are scattered in all directions in the sky. As a result, the all-sky MIR survey performed by the Wide-field Infrared Survey Explorer (WISE; Wright et al. 2010) has uncovered most of the  $\sim 50$  objects that are known or suspected to be Y dwarfs (Cushing et al. 2011, 2014; Kirkpatrick et al. 2012, 2013;

Tinney et al. 2012, 2018; Luhman 2014b; Pinfield et al. 2014; Schneider et al. 2015; Marocco et al. 2019, 2020; Bardalez Gagliuffi et al. 2020; Meisner et al. 2020a, 2020b; Robbins et al. 2023),<sup>13</sup> although a few have been found through companion surveys with the Spitzer Space Telescope (Werner et al. 2004; Luhman et al. 2011, 2012), ground-based NIR adaptive optics imaging (Liu et al. 2011, 2012; Dupuy et al. 2015), and the James Webb Space Telescope (JWST; Calissendorff et al. 2023; Gardner et al. 2023). These discoveries have been accompanied by the development of atmospheric and evolutionary models for the coldest brown dwarfs and giant planets, which can be tested with observations of Y dwarfs (Burrows et al. 2003; Saumon & Marley 2008; Morley et al. 2012, 2014a, 2014b, 2018; Saumon et al. 2012; Tremblin et al. 2015; Zalesky et al. 2019; Phillips et al. 2020; Marley et al. 2021; Tang et al. 2021; Mang et al. 2022; Mukherjee et al. 2022; Lacy & Burrows 2023).<sup>14</sup>

The coldest known brown dwarf is WISE J085510.83–071442.5 (hereafter WISE 0855). Luhman (2014a) and

\* Based on observations made with the NASA/ESA/CSA James Webb Space Telescope.

<sup>12</sup> Royal Society Dorothy Hodgkin Fellow.

Original content from this work may be used under the terms of the [Creative Commons Attribution 4.0 licence](#). Any further distribution of this work must maintain attribution to the author(s) and the title of the work, journal citation and DOI.

<sup>13</sup> The photometry of Ross 19B indicates that it is near the T/Y boundary (Schneider et al. 2021; Meisner et al. 2023).

<sup>14</sup> Leggett et al. (2021) and Meisner et al. (2023) included modified versions of the models from Tremblin et al. (2015) and Phillips et al. (2020).

Kirkpatrick et al. (2014) identified it as a high proper motion object using two epochs of images from WISE. By obtaining images at two additional epochs with Spitzer and measuring its parallax, Luhman (2014b) demonstrated that WISE 0855 is a nearby brown dwarf (the fourth closest known system) and estimated a temperature of  $\sim 250$  K from its absolute magnitude at  $4.5 \mu\text{m}$ . The distance of WISE 0855 has been further refined through continued astrometric monitoring with Spitzer, the reactivated WISE mission (NEOWISE; Mainzer et al. 2014), and the Hubble Space Telescope (HST;  $2.278 \pm 0.012$  pc; Luhman & Esplin 2014, 2016; Wright et al. 2014; Kirkpatrick et al. 2019, 2021). In an effort to measure its spectral energy distribution (SED) for comparison to models of Y dwarfs, deep optical and NIR imaging has been performed on WISE 0855 with HST and large ground-based telescopes (Beamin et al. 2014; Faherty et al. 2014; Kopytova et al. 2014; Luhman 2014b; Wright et al. 2014; Luhman & Esplin 2016; Schneider et al. 2016; Zapatero Osorio et al. 2016; Leggett et al. 2017). NIR spectroscopy of WISE 0855 is not feasible with these facilities, but through very long exposure times with Gemini Observatory, Skemer et al. (2016) and Morley et al. (2018) were able to obtain spectra within portions of the MIR (the *L* and *M* bands) where the atmosphere is not opaque.

JWST is the most sensitive IR telescope deployed to date and operates across a wavelength range that should encompass most of the flux emitted by Y dwarfs. Therefore, it is the ideal facility for measuring the SEDs of Y dwarfs like WISE 0855 (Beiler et al. 2023). In fact, given its status as both the coldest known brown dwarf and the fourth closest known system, as well as the limited ability of other telescopes to observe it, WISE 0855 is one of the most appealing targets of any kind for JWST. In this paper, we present spectroscopy of WISE 0855 from  $0.8$  to  $5.5 \mu\text{m}$  performed with the Near-Infrared Spectrograph (NIRSpec; Jakobsen et al. 2022) on JWST.

## 2. Observations

WISE 0855 was observed with NIRSpec through Guaranteed Time Observation (GTO) program 1230 (PI: C. Alves de Oliveira) on 2023 April 17 (UT). After slewing to WISE 0855, wide aperture target acquisition (WATA) was performed, which employs the S1600A1 aperture ( $1''.6 \times 1''.6$ ). We used a combination of filter (CLEAR), readout pattern (NRSRAPID), and subarray (SUB2048) that would produce a suitable signal-to-noise ratio (S/N) for acquisition given the SED of WISE 0855 (Luhman & Esplin 2016). Through WATA, the centroid of the target was measured, a small angle maneuver was performed to center it in S1600A1, and an offset was applied to place the target in the S200A1 fixed slit, which has an angular size of  $3''.2 \times 0''.2$ . One set of data was collected with the G395M grating, the F290LP filter, the NRSRAPID readout pattern, 840 groups per integration, one integration per nod, and three nod positions. A second data set was taken with the PRISM disperser, the CLEAR filter, the NRSRAPID readout pattern, 1083 groups per integration, three integrations per nod, and three nod positions. Both observations employed the SUBS200A1 subarray. The total exposure times with these configurations were 3931 and 15,200 s, respectively.

## 3. Data Reduction

The data reduction began with the retrieval of the `uncal` files from the Mikulski Archive for Space Telescopes (MAST),

doi:10.17909/1fsf-6j64. We performed ramps-to-slopes processing on those files using a custom pipeline developed by the European Space Agency NIRSpec science operations team, which adopts the same algorithms included in the official STScI pipeline (Alves de Oliveira et al. 2018; Ferruit et al. 2022), except for a correction for “snowballs” (Böker et al. 2023) and a correction for residual correlated noise that is based on unilluminated pixels in the subarray outside the spectral trace (Espinoza et al. 2023). For the PRISM data, which had multiple integrations, we adopted the median of the individual integration count rate maps at each nod position. The median count rate map for each nod was background subtracted using the averaged rate maps of the other two nods and flat-fielded. Spectra were extracted for the individual nod positions and combined with outlier rejection. The same processing steps were performed for standard stars Gaia DR3 2260019315938461952 and Gaia DR3 1634280312200704768 in G395M and PRISM, respectively, which were observed during JWST commissioning through program 1128 (PI: N. Lützgendorf). The spectra of these stars and their flux models (Bohlin et al. 2014)<sup>15</sup> were used for an initial flux calibration of the spectra of WISE 0855. The flux calibrations were then adjusted so that they agree with photometry from Spitzer (Section 4.1). The reduced spectra have sufficient S/Ns to be useful at  $2.87\text{--}5.09$  and  $5.37\text{--}5.54 \mu\text{m}$  (G395M) and  $0.77\text{--}5.53 \mu\text{m}$  (PRISM). The gap in the G395M data is from the separation between the two detector arrays. Our reduction yielded the widest possible wavelength coverage, extending slightly beyond the nominal “science range” officially supported by the STScI pipeline, while ensuring spectrophotometric calibration. The spectral resolution is  $\sim 1000$  for G395M and ranges from  $\sim 40$  near  $1.1 \mu\text{m}$  to  $\sim 300$  at the longest wavelengths for the PRISM disperser.

## 4. Analysis

### 4.1. Comparison to Previous Observations

We compare the NIRSpec data to previous observations of WISE 0855 between  $1$  and  $5 \mu\text{m}$ . We first consider the photometric measurements with the smallest errors, consisting of data in the following filters: the F105W, F110W, F127M, and F160W bands on HST’s Wide Field Camera 3 (WFC3; Kimble et al. 2008) measured by Luhman & Esplin (2016) and Schneider et al. (2016), the [3.6] and [4.5] bands of Spitzer measured by Luhman & Esplin (2016), and W2 from the NEOWISE-R Single Exposure Source Table (Cutri et al. 2023), which contains 18 epochs for WISE 0855 between 2014 and 2022. Each of the NEOWISE epochs consisted of  $\sim 10\text{--}20$  measurements that span a few days. For each epoch, we calculated the median and standard error of W2. We exclude the two epochs from the original WISE survey in 2010 since the photometry of WISE 0855 was contaminated by emission from background stars (Luhman 2014b). For bands that have multiple epochs of photometry with the exception of [3.6], we adopt the midpoint of the measurements and an uncertainty that is represented by the range spanned by those measurements and their errors. The mean, median, and midpoint are nearly identical for [4.5], and the same is true for W2 as well. The adopted values of [4.5] and W2 are  $13.87 \pm 0.08$  and  $13.90 \pm 0.16$ , respectively. Since [3.6] was measured in only four of the nine [4.5] epochs from Luhman & Esplin (2016), we

<sup>15</sup> <https://www.stsci.edu/hst/instrumentation/reference-data-for-calibration-and-tools/astromical-catalogs/calspec>

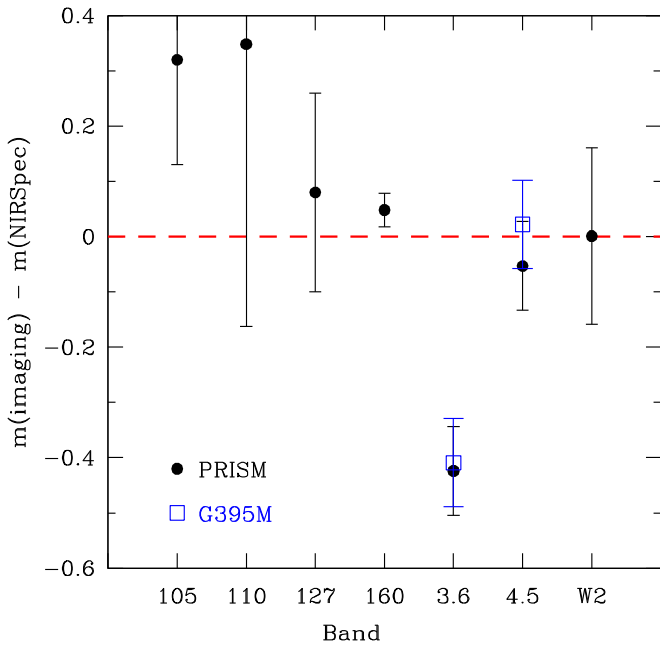


**Figure 1.** Differences between previous photometry from images of WISE 0855 and synthetic photometry measured from NIRSpec PRISM and G395M spectra.

have calculated the weighted mean of the  $[3.6] - [4.5]$  colors among those four epochs (3.49) and applied it to the adopted measurement of  $[4.5]$  to arrive at our adopted value for  $[3.6]$ . The uncertainty for  $[4.5]$  is also assigned to  $[3.6]$ .

We have calculated synthetic Vega magnitudes in the aforementioned bands from the NIRSpec PRISM spectrum of WISE 0855. In addition, photometry has been derived from the G395M spectrum in the two bands that it fully covers,  $[3.6]$  and  $[4.5]$ . These calculations were performed by convolving the spectra of WISE 0855 and a spectrum of Sirius (Rieke et al. 2023) with the photon-counting spectral responses of the filters (Hora et al. 2008; Jarrett et al. 2011; Krick et al. 2021),<sup>16</sup> integrating the resulting fluxes in photons, and assuming that Sirius has a magnitude of  $-1.395$  in each band.

In Figure 1, we have plotted the differences between the imaging and synthetic photometry. For most bands, the synthetic photometry falls within the range of previous measurements. The primary exception is  $[3.6]$ , which is much fainter ( $\sim 0.4$  mag) in both NIRSpec spectra than in the Spitzer images. The spectra and imaging agree more closely in  $[4.5]$ , which means that  $[3.6] - [4.5]$  is redder in the spectra than in the images. To investigate this discrepancy further, we have derived synthetic  $[3.6]$  and  $[4.5]$  for the one other Y dwarf with an available NIRSpec PRISM spectrum, WISE J035934.06  $-$  540154.6 (hereafter WISE 0359; Beiler et al. 2023). We find that its color from NIRSpec is 0.28 mag redder than the value measured with Spitzer (Kirkpatrick et al. 2012), resembling the result for WISE 0855. We also have compared the synthetic and imaging colors in  $W2 - [4.5]$  for these Y dwarfs. The PRISM data indicate  $W2 - [4.5] = -0.02$  for both WISE 0855 and WISE 0359 whereas Spitzer and WISE/NEOWISE have measured 0.03 and 0.06, respectively. It would be useful to perform similar comparisons for a larger sample of T and Y dwarfs observed by NIRSpec.

<sup>16</sup> <https://www.stsci.edu/hst/instrumentation/wfc3/performance/throughputs>

The differences between synthetic and imaging values of  $[3.6] - [4.5]$  and  $W2 - [4.5]$  for WISE 0855 and WISE 0359 could be caused by errors in the filter response functions or variability, although neither Y dwarf has shown large enough variability to explain the discrepancies in  $[3.6]$ , as discussed earlier in this section and elsewhere (Esplin et al. 2016; Brooks et al. 2023). Synthetic  $[3.6]$  photometry for T and Y dwarfs is particularly sensitive to errors in the response function since their fluxes vary significantly across the bandpass, which overlaps with the fundamental band of  $\text{CH}_4$ . The response functions for the IRAC filters do shift slightly in wavelength with position on the detector arrays (Hora et al. 2008). For the  $[3.6]$  band, the maximum redward shift relative to the average response function that we have adopted is  $\sim 80 \text{ \AA}$ , but we find that a shift of  $\sim 500 \text{ \AA}$  would be needed to account for the discrepancy in the photometry. An error in the response function could partially explain why synthetic values of  $[3.6] - [4.5]$  from model spectra for Y dwarfs are redder than observed colors (Leggett et al. 2021).

Among the bands that we have discussed,  $[4.5]$  is the best one for refining the flux calibrations of the PRISM and G395M spectra of WISE 0855 since it contains a large fraction of the flux in those data, is fully encompassed by both spectra, and has the most accurate photometry available from previous imaging. Based on their synthetic photometry, the PRISM spectrum is 0.053 mag fainter and the G395M spectrum is 0.022 mag brighter than our adopted photometry of  $[4.5] = 13.87$ . We have elected to multiply the spectra by the appropriate factors to bring them into agreement with the latter. Doing so results in a modest discrepancy of  $\sim 0.1$  mag between synthetic and imaging photometry in F160W, which could be explained by variability.

Skemer et al. (2016) and Morley et al. (2018) obtained  $M$ - and  $L$ -band spectra, respectively, of WISE 0855 with the Gemini Near-Infrared Spectrograph (GNIRS; Elias et al. 2006). An updated reduction of the data from Skemer et al. (2016) was presented by Miles et al. (2020). The data were binned to resolutions of  $\sim 250$  ( $L$ ) and  $\sim 300$  ( $M$ ), after which they had median S/Ns of  $\sim 5$  ( $L$ ) and 13 ( $M$ ). In Figure 2, we compare the binned spectra from Morley et al. (2018) and Miles et al. (2020) to the NIRSpec PRISM spectrum, which has a similar resolution. The errors in the NIRSpec fluxes are not plotted since most are too small to be distinguishable from the spectrum. The GNIRS and NIRSpec spectra have similar spectral slopes and show many of the same absorption features, although the strengths of some of the features differ by substantially more than  $1\sigma$ .

#### 4.2. Spectral Features

The NIRSpec spectra of WISE 0855 are presented in Figures 3 and 4 (PRISM and G395M). The spectra are available in electronic files associated with those figures. Since the fluxes span a very large range, the spectra are shown on both linear and logarithmic flux scales. Fluxes that are consistent with zero at  $1\sigma$  are not plotted. Given that the fluxes vary significantly with wavelength, the S/Ns do so as well. In the fainter half of the PRISM spectrum ( $< 2.5 \mu\text{m}$ ), the brightest 50% of pixels have a median S/N of  $\sim 20$  while no significant flux is detected in the strongest absorption bands. At the wavelengths of that half of the PRISM spectrum, only photometry (usually with low S/N) has been available from previous observations (Section 4.1). The brightest fluxes in the

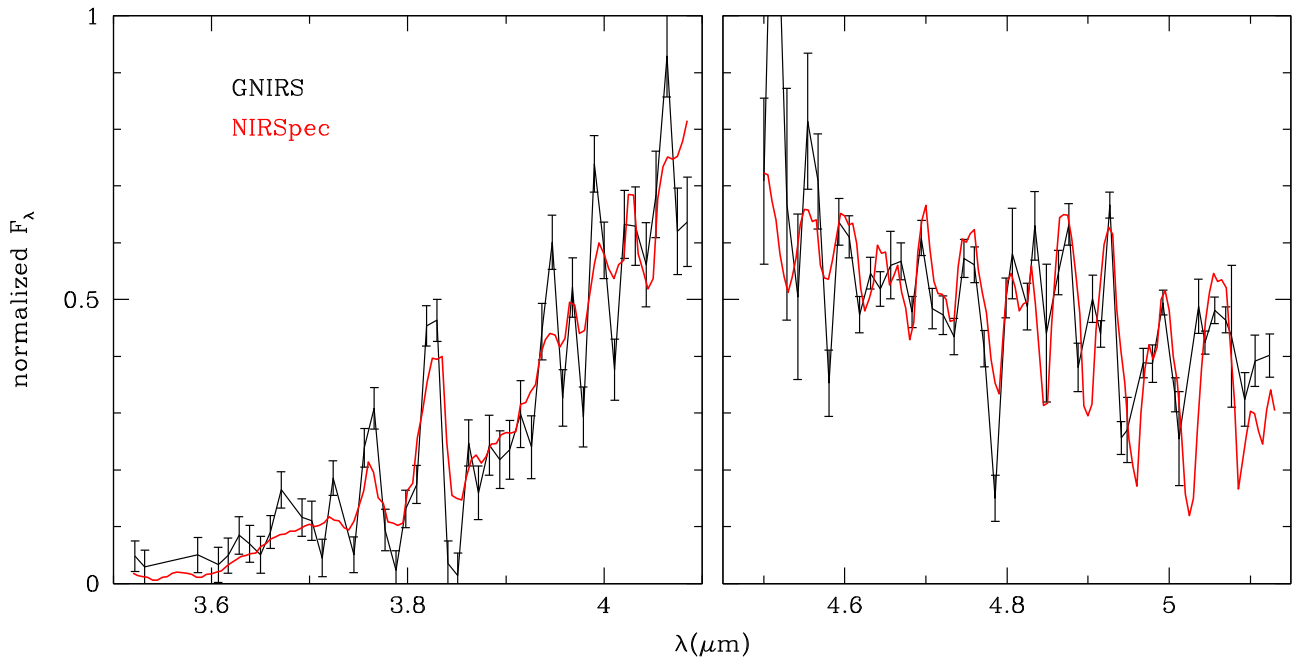


**Figure 2.** Comparison of spectra for WISE 0855 from Gemini/GNIRS (Skemer et al. 2016; Morley et al. 2018; Miles et al. 2020) and JWST/NIRSpec (this work).

PRISM data are at 4–5  $\mu\text{m}$ , where the median S/N is  $\sim 90$ . Given their S/Ns, wavelength coverage, and spectral resolution (for G395M), the NIRSpec data have provided a dramatic improvement in the characterization of the SED of WISE 0855.

The SED of WISE 0855 is shaped by absorption from several molecular species. In the bottom panels of Figures 3 and 4, we have plotted a representation of the opacities for the dominant absorbers that are expected in Y dwarfs, consisting of  $\text{H}_2\text{O}$ ,  $\text{CH}_4$ ,  $\text{NH}_3$ ,  $\text{CO}$ ,  $\text{CO}_2$ , and  $\text{PH}_3$  as well as collision-induced absorption (CIA) of  $\text{H}_2$  and He. In those opacity diagrams, the vertical thickness of each band is proportional to the logarithm of the abundance-weighted absorption cross section for a given molecule at  $P = 1$  bar and  $T_{\text{eff}} = 250$  K based on the model of WISE 0855 from Leggett et al. (2021). We have summed the abundance-weighted cross sections for the CIA absorption of  $\text{H}_2$  and He. For the model in question, the opacities of  $\text{CO}_2$ ,  $\text{CO}$ , and  $\text{PH}_3$  are much smaller than those of the other species, so for the purposes of Figures 3 and 4, we have scaled the opacities of  $\text{CO}_2$ ,  $\text{CO}$ , and  $\text{PH}_3$  by factors of 1000, 100, and 1000, respectively.

For comparison to WISE 0855, we have included in Figure 3 the NIRSpec PRISM spectrum of WISE 0359 (Beiler et al. 2023), which has a spectral type of Y0 (Kirkpatrick et al. 2012). The data for WISE 0359 have been scaled to roughly match the fluxes of WISE 0855 at 4–5  $\mu\text{m}$ . WISE 0359 is bluer from NIR to MIR wavelengths than WISE 0855, which reflects its earlier spectral type and higher temperature ( $\sim 450$  K; Beiler et al. 2023). WISE 0359 has strong absorption from  $\text{CO}_2$  and  $\text{CO}$  at 4–5  $\mu\text{m}$ , whereas WISE 0855 lacks  $\text{CO}_2$  and has much weaker  $\text{CO}$  (Miles et al. 2020; Section 4.5). Beiler et al. (2023) noted the detection of a relatively narrow feature at 3  $\mu\text{m}$  in WISE 0359, which they attributed to the Q branch of the  $\nu_1$  band of  $\text{NH}_3$ . That feature is detected in WISE 0855 as well.

#### 4.3. Spectral Classification

Most known Y dwarfs have been classified as Y0 or Y1 (Kirkpatrick et al. 2021). One Y dwarf, WISEPA J182831.08

+265037.8, has a spectral type of  $\geq Y2$  (Kirkpatrick et al. 2012). WISE 0855 is the one remaining Y dwarf, which has been assigned a tentative classification of Y4 based on its colors and absolute magnitudes (Kirkpatrick et al. 2019, 2021). NIRSpec has provided the first spectrum of WISE 0855 that is suitable for spectral classification. Those data are consistent with an effective temperature that is significantly cooler than those of other known Y dwarfs (Figure 3, Section 4.5), so Y4 remains a reasonable choice for its spectral type. The definition of classes later than Y1 will require JWST spectra of a larger sample of the coolest known Y dwarfs (e.g., JWST program 2302, PI: M. Cushing) and would be facilitated by the discovery of objects that more closely approach the temperature of WISE 0855.

#### 4.4. Previous Comparisons to Models

Previous studies have compared photometry and spectroscopy of WISE 0855 to the predictions of atmospheric models in an attempt to characterize its atmosphere and test the models. Such models are categorized in part based on whether they assume chemical equilibrium or nonequilibrium chemistry due to vertical mixing, and whether they assume clear or cloudy atmospheres. Warmer Y dwarfs may have sulfide clouds (Morley et al. 2012) and show evidence of nonequilibrium chemistry (Cushing et al. 2011; Miles et al. 2020; Leggett et al. 2021; Beiler et al. 2023). A brown dwarf as cold as WISE 0855 is expected to have clouds of  $\text{H}_2\text{O}$  ice ( $< 350$  K; Burrows et al. 2003; Morley et al. 2014b) and could experience nonequilibrium chemistry given its presence in the atmosphere of Jupiter (Prinn & Lewis 1975; Visscher et al. 2006).

Early studies of WISE 0855 found that its photometric SED was poorly matched by all of the models from available grids and did not favor one model prescription over another (e.g., cloudless versus cloudy; Luhman & Esplin 2014, 2016; Schneider et al. 2016; Leggett et al. 2017). Photometric monitoring with Spitzer has measured the MIR variability of WISE 0855, which is similar to that of warmer Y dwarfs and is

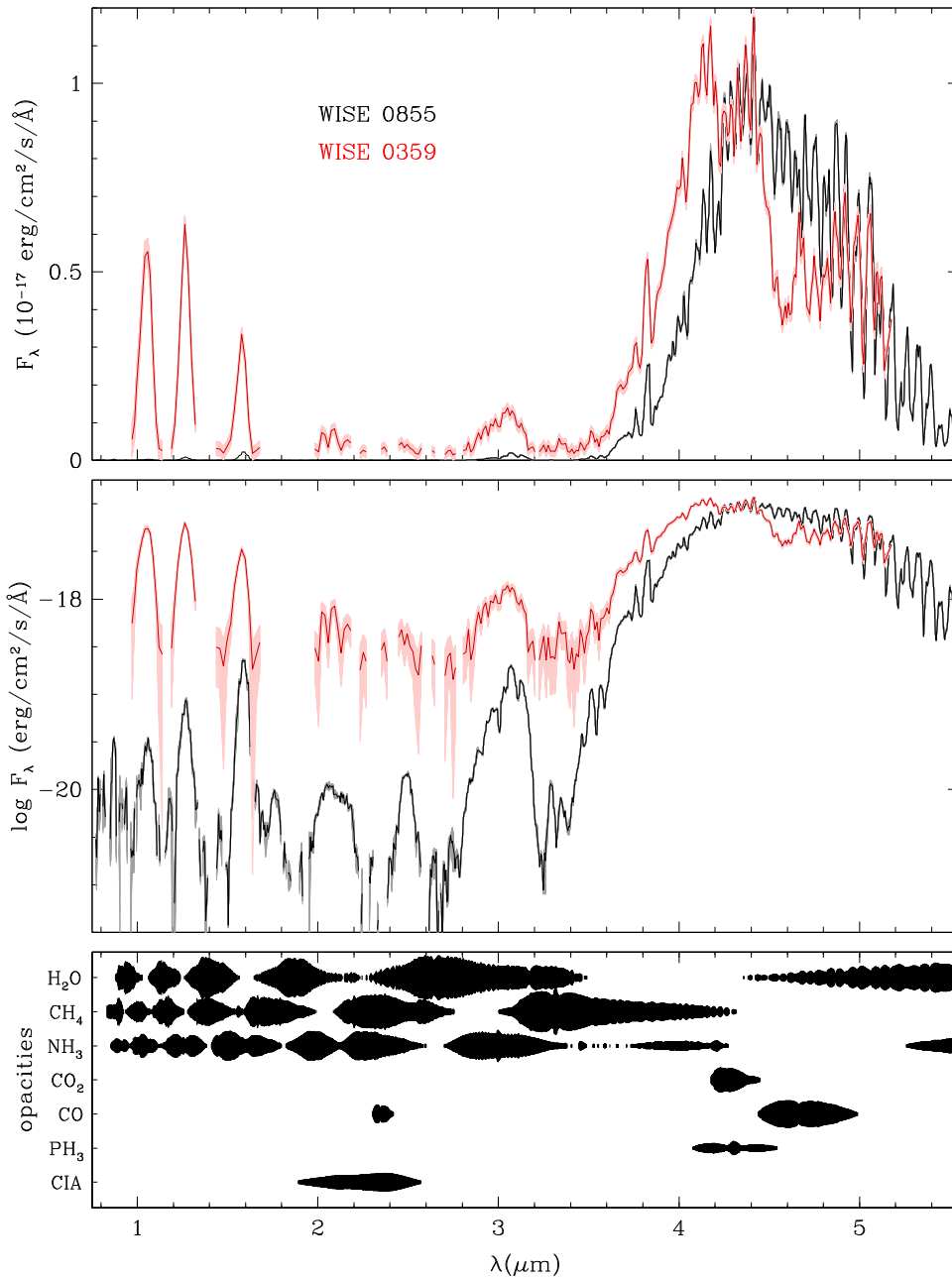


**Figure 3.** NIRSpect PRISM spectra of WISE 0855 (this work) and the Y0 dwarf WISE 0359 (Beiler et al. 2023) on linear and logarithmic flux scales (top and middle). The spectrum of WISE 0359 has been scaled to roughly match the data for WISE 0855 at 4–5  $\mu\text{m}$ . Uncertainties of  $\pm 1\sigma$  are plotted as gray and pink bands. Fluxes that are consistent with zero ( $F_\lambda - \sigma \leq 0$ ) have been omitted. The bottom panel shows a representation of opacities in which the vertical thickness of each band is proportional to the logarithm of the abundance-weighted absorption cross section for a given molecule at  $P = 1$  bar and  $T_{\text{eff}} = 250$  K (bottom). The opacities of  $\text{CO}_2$ ,  $\text{CO}$ , and  $\text{PH}_3$  have been scaled by factors of 1000, 100, and 1000, respectively, so that their strongest features are visible.

(The data used to create this figure are available.)

inconclusive regarding the presence of  $\text{H}_2\text{O}$  ice clouds (Esplin et al. 2016). Skemer et al. (2016), Morley et al. (2018), and Miles et al. (2020) found that cloudy models provided a better match to their  $M$ -band spectra than cloudless models, which was cited as evidence of  $\text{H}_2\text{O}$  clouds. However, given the untested nature of models in the temperature regime of WISE 0855, if one model prescription appears to be favored by data in a limited range of wavelengths, the same may not be true at other wavelengths or with other suites of models. Indeed, the cloudy models from those studies were discrepant in multiple bands of the photometric SED while

Leggett et al. (2021) were able to use cloudless models (Phillips et al. 2020) to simultaneously reproduce the slopes of the  $L/M$ -band spectra and provide a good fit to the SED. Meanwhile, detections of  $\text{PH}_3$  and  $\text{CO}$  would be two of the most obvious signatures of nonequilibrium chemistry. The former was not detected in the  $L/M$ -band spectra (Skemer et al. 2016; Morley et al. 2018; Miles et al. 2020), but Miles et al. (2020) reported the presence of weak  $\text{CO}$  absorption in the  $M$ -band spectrum. In their modeling of the SED of WISE 0855, Lacy & Burrows (2023) found that models with clouds and equilibrium chemistry provided the best fit.

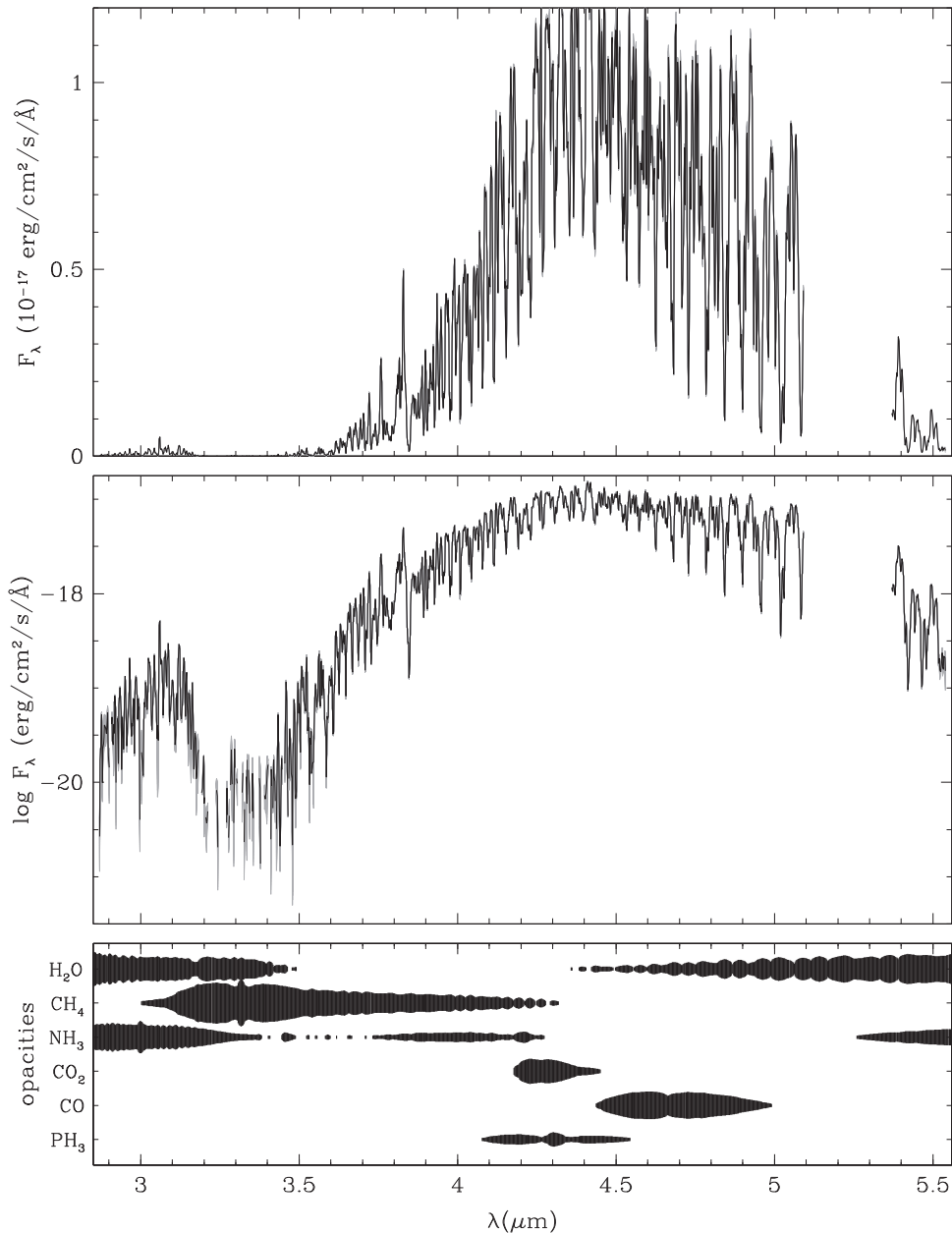


**Figure 4.** NIRSpect G395M spectrum of WISE 0855 on linear and logarithmic flux scales (top and middle). Uncertainties of  $\pm 1\sigma$  are plotted as gray bands. Fluxes that are consistent with zero ( $F_\lambda - \sigma \leq 0$ ) have been omitted. The bottom panel shows the opacities from Figure 3.

(The data used to create this figure are available.)

Given that the SED of WISE 0855 has been sampled sparsely and typically with low S/Ns, and given the degeneracies and uncertainties in the model spectra, it has been unclear from modeling of previous data whether the atmosphere of WISE 0855 experiences H<sub>2</sub>O ice clouds or nonequilibrium chemistry.

#### 4.5. Comparison of the NIRSpect Data to Models

In an initial attempt at modeling the NIRSpect data for WISE 0855, we have searched for model spectra that reproduce the PRISM data from among available grids that are defined by the following features: cloudless atmospheres with either chemical equilibrium and nonequilibrium chemistry (ATMO 2020; Tremblin et al. 2015; Phillips et al. 2020; Leggett et al. 2021; Meisner et al. 2023), cloudless atmospheres and chemical

equilibrium (Sonora Bobcat; Marley et al. 2021), cloudless atmospheres and nonequilibrium chemistry (Saumon et al. 2012), partly cloudy atmospheres and chemical equilibrium (Morley et al. 2012, 2014b), and cloudy and cloudless atmospheres with chemical equilibrium and nonequilibrium chemistry (Lacy & Burrows 2023). None of the grids provided a sufficiently close match to the PRISM spectrum to be useful.

For all of the model suites that we considered, it is possible that the parameters defining the grids are too sparsely sampled and that a good fit could be achieved with custom models in which the parameters are tuned for WISE 0855. We have performed such an exercise with the ATMO 2020 models for both chemical equilibrium and nonequilibrium chemistry. As an initial model, we adopted the one for WISE 0855 from

Leggett et al. (2021), which had  $T_{\text{eff}} = 260$  K, a surface gravity of  $\log g = 4$  [ $\text{cm s}^{-2}$ ], an eddy diffusion coefficient of  $K_{\text{zz}} = 10^{8.7}$ , an effective adiabatic index of  $\gamma = 1.33$ , and solar values for metallicity and C/O. We then increased the effective temperature to improve the fit at 2–4  $\mu\text{m}$ , scaled all fluxes downward to maintain agreement near 4.5–5  $\mu\text{m}$  (i.e., decreased the radius), and decreased  $\gamma$  to further improve the fit at  $< 3$   $\mu\text{m}$ . The resulting model, which we refer to as the “base model,” has  $T_{\text{eff}} = 285$  K and  $\gamma = 1.3$  while the remaining parameters are unchanged from the model in Leggett et al. (2021).

In Figure 5, we show a portion of the G395M spectrum that includes bands from  $\text{PH}_3$ ,  $\text{NH}_3$ , and CO. The top panel compares the data to the spectrum from our base model. The prescription for nonequilibrium chemistry in that model produces mixing ratios of  $7.7 \times 10^{-5}$  for  $\text{NH}_3$  and  $2 \times 10^{-7}$  for CO. The model does not account for mixing of  $\text{PH}_3$ , and instead uses the mixing ratio of  $5 \times 10^{-7}$  derived for chemical equilibrium (Phillips et al. 2020; Leggett et al. 2021). The strongest features from  $\text{NH}_3$  and  $\text{PH}_3$  are evident in the model spectrum at 4.2 and 4.3  $\mu\text{m}$ , respectively. Additional absorption at other wavelengths from  $\text{PH}_3$  and CO is present in the model, but it does not appear as well-defined features against the backdrop of  $\text{CH}_4$  and  $\text{H}_2\text{O}$  bands.

To illustrate the influence of  $\text{PH}_3$  and CO on the model spectra, we show in Figure 5 modified versions of the base model after removing the opacities of  $\text{PH}_3$ , removing both  $\text{PH}_3$  and CO, and reducing the mixing ratio of  $\text{PH}_3$  to  $10^{-8}$ . For each of these models, the pressure–temperature profile was reconverged to maintain hydrostatic and energy equilibria. The model with no  $\text{PH}_3$  agrees well with the data near the wavelength of the strongest feature of  $\text{PH}_3$  (4.3  $\mu\text{m}$ ), indicating that  $\text{PH}_3$  is not detected. The model that lacks both  $\text{PH}_3$  and CO is significantly brighter than the data across the wavelength range of CO (4.5–4.9  $\mu\text{m}$ ), demonstrating that CO is clearly detected. Meanwhile, the spectrum in that range is well matched by the base model. The mixing ratio of CO in the base model is similar to the value derived by Miles et al. (2020) from modeling of the ground-based  $M$ -band spectrum obtained by Skemer et al. (2016). In the model with a reduced mixing ratio of  $10^{-8}$  for  $\text{PH}_3$ , the 4.3  $\mu\text{m}$  feature is weak but detectable, which provides a rough upper limit on the abundance of that species. In Figure 5, the models in which  $\text{PH}_3$  has been removed or reduced are brighter than the data at 4.3–4.5  $\mu\text{m}$ , which is discussed later in the context of the PRISM data.

As discussed in Miles et al. (2020), the detection of CO in WISE 0855 indicates the presence of nonequilibrium chemistry due to vertical mixing. The degree of vertical mixing needed to account for the observed CO absorption in WISE 0855 is expected to produce strong  $\text{PH}_3$  as well, but it is not detected. Like WISE 0855, the Y dwarf WISE 0359 exhibits absorption in CO but not  $\text{PH}_3$  in its NIRSpect data (Beiler et al. 2023).

In Figure 6, we compare the PRISM data to the spectra produced by the base model and the modified version with  $\text{PH}_3$  removed, which provided the best match to the G395M spectrum. When normalizing the model to the data at 4.5–5  $\mu\text{m}$  as we have done, the model agrees with the data at 0.8–1.6  $\mu\text{m}$ , is too faint at 1.6–4 and 5–5.6  $\mu\text{m}$ , and is too bright at 4.3–4.5  $\mu\text{m}$  (see also Figure 5). It is possible that the fit could be improved by adjusting the abundances of some of the dominant absorbers. For instance, the abundance of  $\text{NH}_3$  in our

model may need to be reduced based on the strength of the 4.2  $\mu\text{m}$  absorption feature (Figure 5). The source of the discrepancy at 4.3–4.5  $\mu\text{m}$  is unclear. We note that this wavelength range corresponds to the minimum in the opacities of the dominant absorbers (Figure 6).

The temperature for our best model for WISE 0855 (285 K) is somewhat higher than the value of 253–276 K derived by combining our luminosity estimate with the luminosities predicted by evolutionary models (Section 4.6). As an alternative illustration of the difference, the model temperature combined with our luminosity estimate correspond to a radius of 0.092  $R_{\odot}$ , which is smaller than the radii of 0.10–0.11  $R_{\odot}$  that are predicted by evolutionary models for brown dwarfs at the luminosity of WISE 0855 for ages of 1–10 Gyr.

As mentioned in Section 4.1, Skemer et al. (2016), Morley et al. (2018), and Miles et al. (2020) found that their ground-based  $M$ -band spectrum of WISE 0855 was better matched by cloudy models than cloudless models, which was cited as evidence of  $\text{H}_2\text{O}$  ice clouds. However, the spectrum produced by our cloudless model agrees well with the NIRSpect data in that wavelength range (Figure 5).

Future studies can improve upon our modeling of WISE 0855 by incorporating 5–28  $\mu\text{m}$  data that were collected with the Mid-infrared Instrument (MIRI; Rieke et al. 2015) on JWST during the same visit as the NIRSpect observations, optimizing the abundances of the dominant absorbers in cloudless models like those from ATMO 2020, tuning the latest cloudy models to fit WISE 0855 (Lacy & Burrows 2023), and performing retrieval analysis (Birmingham et al. 2017; Line et al. 2017; Zalesky et al. 2019; Rowland et al. 2023).

#### 4.6. Luminosity Estimate

According to the model spectra for WISE 0855, the NIRSpect PRISM data (0.77–5.53  $\mu\text{m}$ ) should encompass roughly one-third of its total flux. We have estimated the bolometric luminosity of WISE 0855 by integrating the flux in the PRISM spectrum and our 285 K model at shorter and longer wavelengths and applying the parallactic distance measured by Kirkpatrick et al. (2021), arriving at  $\log L/L_{\odot} = -7.305 \pm 0.020$ . This calculation is similar to simply quoting the luminosity of our best-fit model. As mentioned in Section 4.1, the NIRSpect spectra have been flux calibrated using the mean of multiple epochs of photometry at 4.5  $\mu\text{m}$  with Spitzer. We have adopted the standard deviation of those measurements as the uncertainty in the flux calibration. The error in our luminosity estimate does not include the uncertainty in the model flux beyond the wavelength range of the PRISM data. It will be possible to eventually eliminate most of that uncertainty by incorporating the 5–28  $\mu\text{m}$  data from MIRI.

We can estimate the effective temperature of WISE 0855 from its luminosity and the radii predicted by evolutionary models. In Figure 7, we have plotted the luminosity estimate for WISE 0855 with the luminosities as a function of temperature predicted by two sets of evolutionary models for ages of 1 and 10 Gyr, which encompass most members of the solar neighborhood. We have included the luminosity for WISE 0359 from Beiler et al. (2023) for comparison. We have shown models of cloudless atmospheres with chemical equilibrium and solar metallicity (Marley et al. 2021; Chabrier et al. 2023). Very similar luminosities are produced by models with cloudy atmospheres and nonequilibrium chemistry

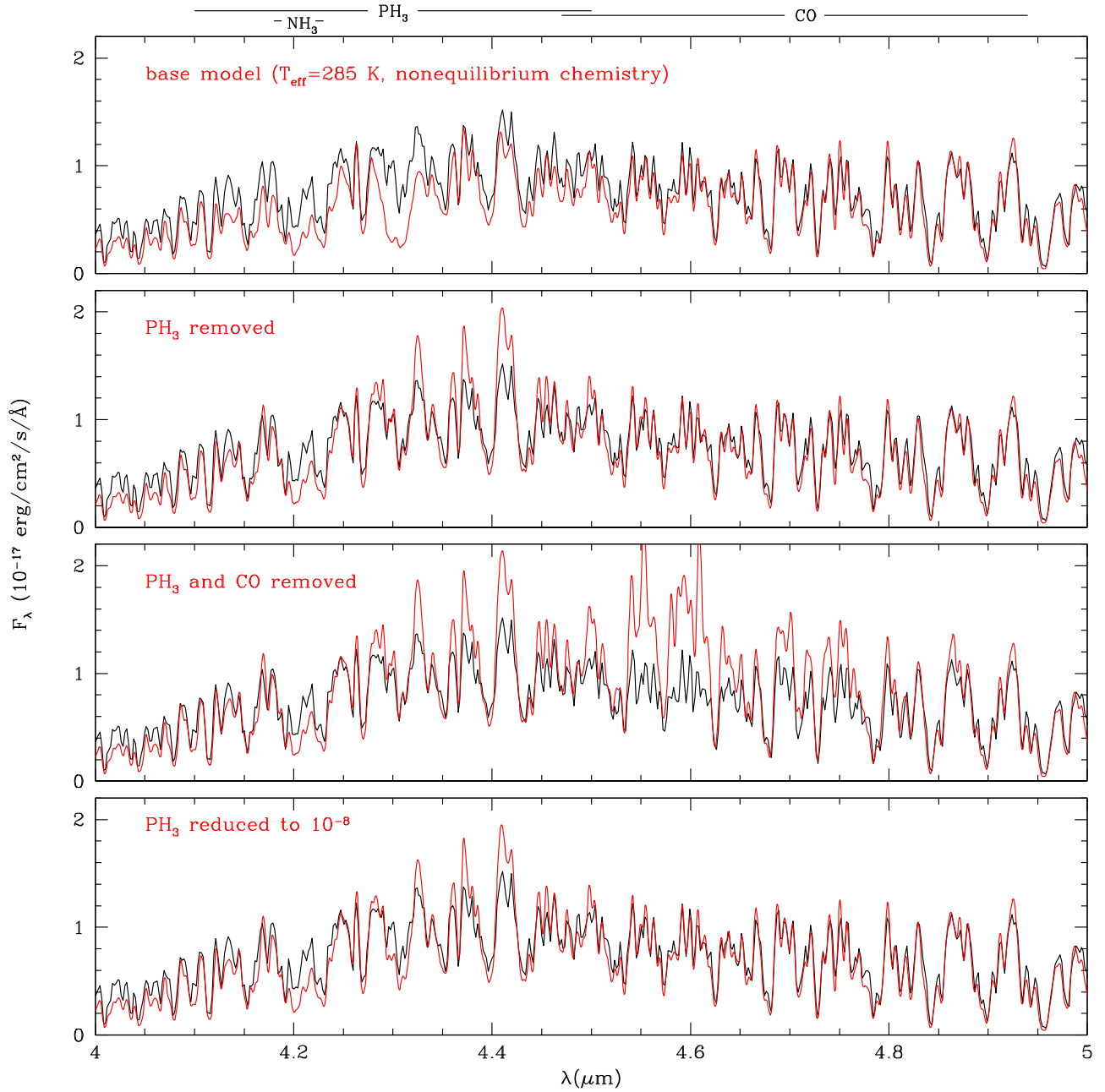


**Figure 5.** NIRSpect G395M spectrum of WISE 0855 compared to spectra produced by models of cloudless atmospheres (Tremblin et al. 2015; Phillips et al. 2020). The top panel shows our base model, which uses  $T_{\text{eff}} = 285$  K and nonequilibrium chemistry. In the remaining panels, we have modified the base model to remove  $\text{PH}_3$ , remove both  $\text{PH}_3$  and  $\text{CO}$ , and reduce the mixing ratio of  $\text{PH}_3$  to  $10^{-8}$ .

(Saumon et al. 2012; Morley et al. 2014b; Chabrier et al. 2023). Based on the evolutionary models, the luminosity of WISE 0855 corresponds to a temperature of 253–276 K for an age of 1–10 Gyr, which is somewhat cooler than the value implied by the model spectra (Section 4.5). As mentioned earlier, the true uncertainty in our luminosity estimate is larger than the value we have quoted and plotted in Figure 7, so the same is true for the temperature estimate.

To illustrate the expected surface gravity of WISE 0855, we have included in Figure 7 a diagram of the predicted luminosities as a function of surface gravity for 1 and 10 Gyr. The luminosity of WISE 0855 is indicative of  $\log g \sim 4$  [ $\text{cm s}^{-2}$ ]. Meanwhile, the luminosity corresponds to a mass range of 3–10  $M_{\text{Jup}}$  for ages of 1–10 Gyr according to the evolutionary models.

## 5. Conclusions

We have used NIRSpect on JWST to perform 1–5  $\mu\text{m}$  spectroscopy on WISE 0855, which is the coldest known brown dwarf. Our results are summarized as follows:

1. We observed WISE 0855 in the fixed slit mode of NIRSpect with the PRISM and G395M dispersers ( $R \sim 40$ –300 and 1000, respectively), which produced useful data at 0.77–5.53  $\mu\text{m}$  and 2.87–5.09/5.37–5.54  $\mu\text{m}$ , respectively. NIRSpect has provided the first spectroscopy of WISE 0855 for most of those wavelengths. Although the brown dwarf is extremely faint at  $<2.5$   $\mu\text{m}$ , the combination of NIRSpect’s sensitivity and the long exposure time for the PRISM data (4.2 hr) has yielded relatively high S/Ns in that wavelength

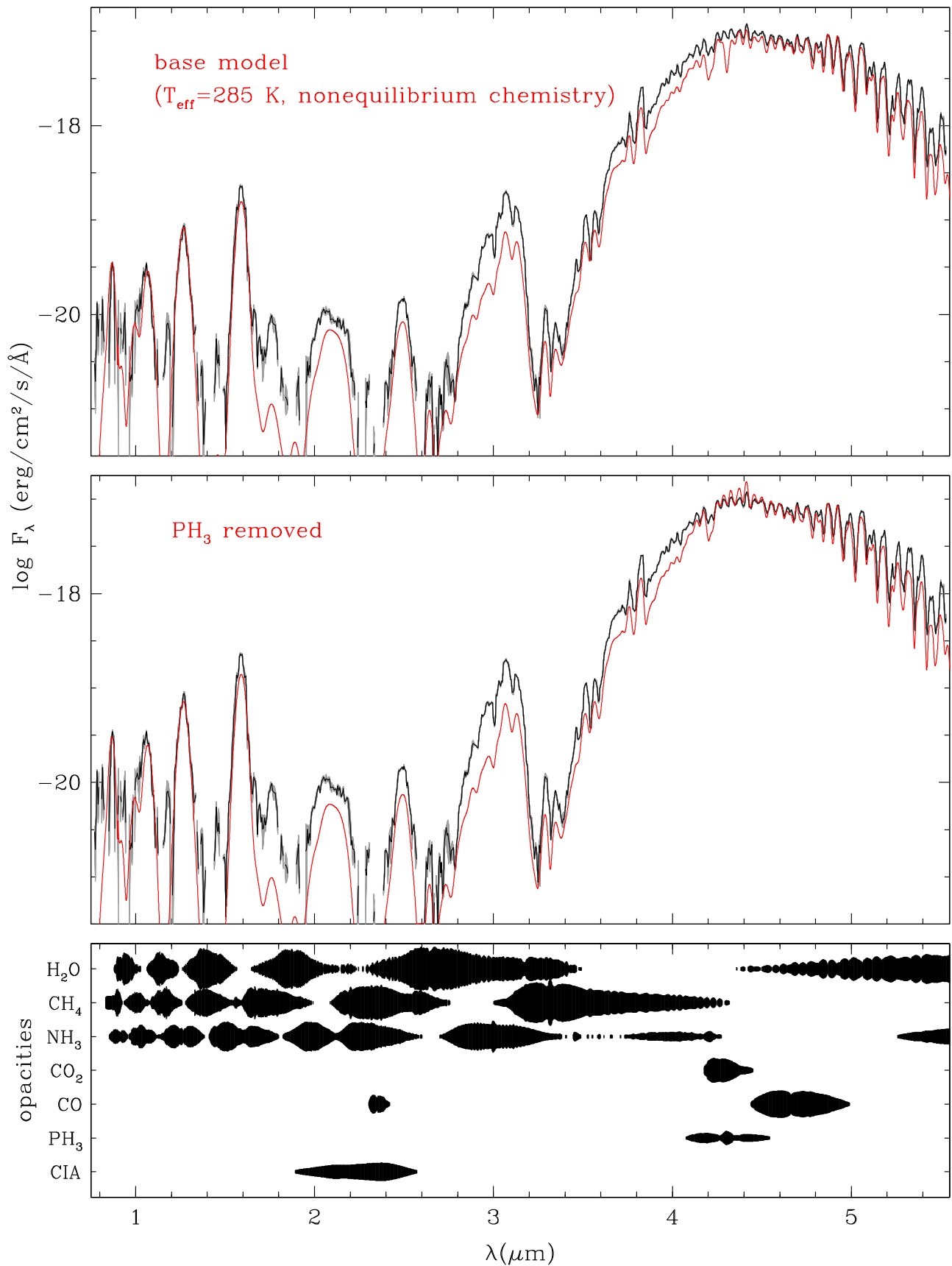


**Figure 6.** NIRSpc PRISM spectrum of WISE 0855 compared to spectra produced by models of cloudless atmospheres (Tremblin et al. 2015; Phillips et al. 2020). The top panel shows our base model for  $T_{\text{eff}} = 285$  K and nonequilibrium chemistry. In the bottom panel, we have modified the base model to remove PH<sub>3</sub>.

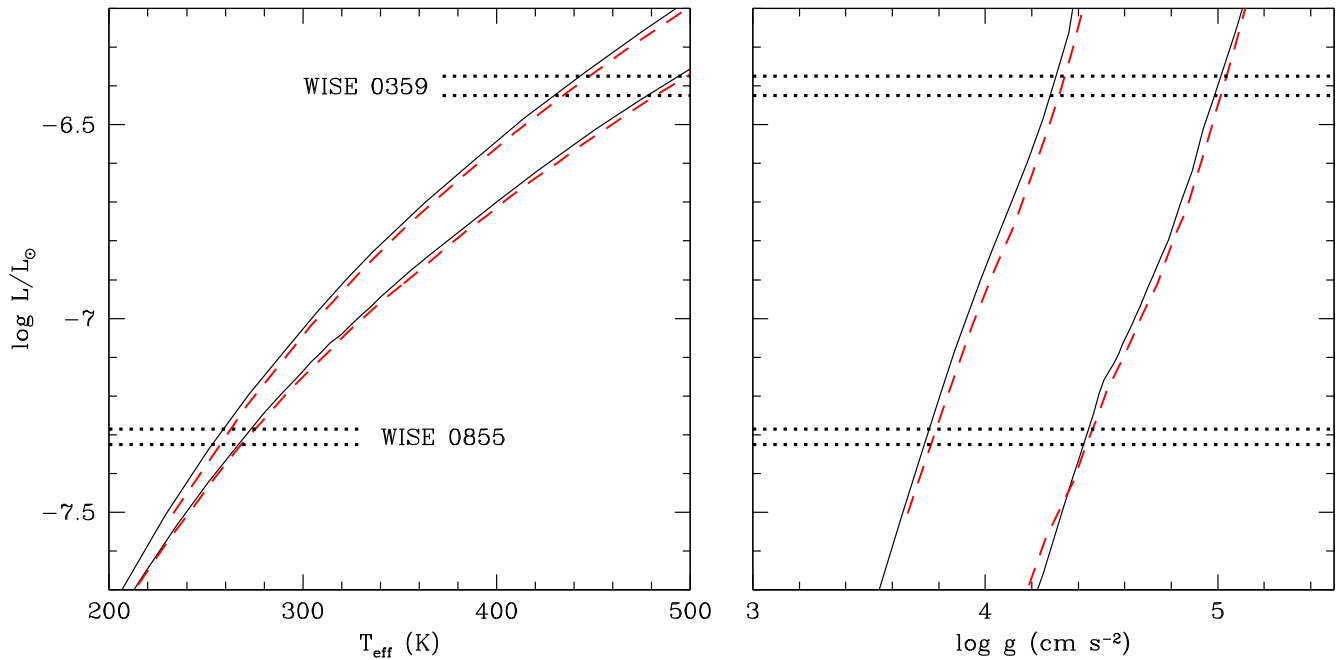


**Figure 7.** Luminosity estimates for WISE 0855 (this work) and WISE 0359 (Beiler et al. 2023) compared to luminosities as a function of temperature and surface gravity predicted for ages for 1 and 10 Gyr by the evolutionary models of Marley et al. (2021; solid lines) and Chabrier et al. (2023; dashed lines).

range, with a median value of  $\sim 20$  for the brightest 50% of pixels (i.e., outside of the deepest bands).

2. We have calculated synthetic photometry from the NIRSpectra in several filters in which photometry has been previously measured. The synthetic and imaging photometry are consistent with each other in most filters with the exception of [3.6] from Spitzer. The synthetic value of [3.6] from NIRSpectra is  $\sim 0.4$  mag fainter than the measurement from Spitzer, which implies that [3.6] – [4.5] is redder in the spectrum than in the images. We find that the NIRSpectra data for the Y0 dwarf WISE 0359 (Beiler et al. 2023) exhibits a similar discrepancy. It would be useful to check whether the discrepancy extends to other T and Y dwarfs observed by NIRSpectra.
3. We have performed preliminary modeling of the NIRSpectra data using the ATMO 2020 models of cloudless atmospheres (Tremblin et al. 2015; Phillips et al. 2020). Our best fitting model has  $T_{\text{eff}} = 285$  K, nonequilibrium chemistry ( $K_{\text{zz}} = 10^{8.7}$ ), an effective adiabatic index of  $\gamma = 1.3$ , and solar metallicity. The modeling demonstrates a clear detection of the fundamental band of CO, which is consistent with an earlier detection by Miles et al. (2020) with ground-based data and indicates the presence of vertical mixing. Previous observations of WISE 0855 and other Y dwarfs have found an absence of PH<sub>3</sub> that seems inconsistent with the vertical mixing implied by other species like CO (Miles et al. 2020; Beiler et al. 2023). Similarly, NIRSpectra does not detect PH<sub>3</sub> in WISE 0855, providing an improved constraint in its mixing ratio ( $< 10^{-8}$ ).
4. The temperature of our best fitting model is  $\sim 20$  K higher than the value derived when our luminosity estimate is combined with evolutionary models (i.e., the radius implied by the fit to the SED is somewhat smaller than expected based on evolutionary models).
5. Previous ground-based *M*-band spectroscopy of WISE 0855 (4.5–5.1  $\mu\text{m}$ ) has been cited for evidence of H<sub>2</sub>O ice clouds, but we find that the NIRSpectra data in that wavelength range

are matched well by our cloudless model. Thus, clear evidence of H<sub>2</sub>O ice clouds in WISE 0855 has not been identified yet, but it may still be present in the NIRSpectra data. The physical properties of WISE 0855, including the presence of H<sub>2</sub>O clouds, can be better constrained with more concerted modeling efforts using both cloudless and cloudy models and the incorporation of 5–28  $\mu\text{m}$  data from MIRI.

### Acknowledgments

We thank Michael Cushing and Samuel Beiler for helpful discussions and Brianna Lacy for providing her model calculations. P.T. acknowledges support from the European Research Council under grant agreement ATMO 757858. R.P. acknowledges support from the Royal Society in the form of a Dorothy Hodgkin Fellowship. The JWST data were obtained from MAST at the Space Telescope Science Institute, which is operated by the Association of Universities for Research in Astronomy, Inc., under NASA contract NAS 5-03127. The JWST observations are associated with program 1230. The Center for Exoplanets and Habitable Worlds is supported by the Pennsylvania State University, the Eberly College of Science, and the Pennsylvania Space Grant Consortium.

### ORCID iDs

K. L. Luhman <https://orcid.org/0000-0003-2822-2951>  
P. Tremblin <https://orcid.org/0000-0001-6172-3403>  
C. Alves de Oliveira <https://orcid.org/0000-0003-2896-4138>  
S. M. Birkmann <https://orcid.org/0000-0001-7058-1726>  
I. Baraffe <https://orcid.org/0000-0001-8365-5982>  
G. Chabrier <https://orcid.org/0000-0002-8342-9149>  
E. Manjavacas <https://orcid.org/0000-0003-0192-6887>  
R. J. Parker <https://orcid.org/0000-0002-1474-7848>  
J. Valenti <https://orcid.org/0000-0003-3305-6281>

## References

- Alves de Oliveira, C., Birkmann, S. M., Böker, T., et al. 2018, *Proc. SPIE*, **10704**, 107040Q
- Bardalez Gagliuffi, D. C., Faherty, J. K., Schneider, A. C., et al. 2020, *ApJ*, **895**, 145
- Beamin, J. C., Ivanov, V. D., Bayo, A., et al. 2014, *A&A*, **570**, L8
- Beiler, S., Cushing, M., Kirkpatrick, J. D., et al. 2023, *ApJL*, **951**, L48
- Bohlin, R. C., Gordon, K. D., & Tremblay, P.-E. 2014, *PASP*, **126**, 711
- Böker, T., Beck, T. L., Birkmann, S. M., et al. 2023, *PASP*, **135**, 038001
- Brooks, H., Kirkpatrick, J. D., Meisner, A. M., et al. 2023, *AJ*, **165**, 232
- Burningham, B., Marley, M. S., Line, M. R., et al. 2017, *MNRAS*, **470**, 1177
- Burrows, A., Sudarsky, D., & Lunine, J. I. 2003, *ApJ*, **596**, 587
- Calissendorff, P., De Furio, M., Meyer, M., et al. 2023, *ApJL*, **947**, L30
- Chabrier, G., Baraffe, I., Phillips, M., & Debras, F. 2023, *A&A*, **671**, A119
- Cushing, M. C., Kirkpatrick, J. D., Gelino, C. R., et al. 2011, *ApJ*, **743**, 50
- Cushing, M. C., Kirkpatrick, J. D., Gelino, C. R., et al. 2014, *AJ*, **147**, 113
- Cutri, R. M., Mainzer, A., Conrow, T., et al. 2023, NEOWISE-R Single Exposure Source Table, IPAC, doi:[10.26131/IRSA144](https://doi.org/10.26131/IRSA144)
- Dupuy, T. J., Liu, M. C., & Leggett, S. K. 2015, *ApJ*, **803**, 102
- Elias, J. H., Joyce, R. R., Liang, M., et al. 2006, *Proc. SPIE*, **6269**, 62694C
- Espinoza, N., Úbeda, L., Birkmann, S. M., et al. 2023, *PASP*, **135**, 018002
- Esplin, T. L., Luhman, K. L., Cushing, M. C., et al. 2016, *ApJ*, **832**, 58
- Faherty, J. K., Tinney, C. G., Skemer, A., & Monson, A. J. 2014, *ApJL*, **793**, L16
- Ferruit, P., Jakobsen, P., Giardino, G., et al. 2022, *A&A*, **661**, A81
- Gardner, J. P., Mather, J. C., Abbott, R., et al. 2023, *PASP*, **135**, 068001
- Hora, J. L., Carey, S., Surace, J., et al. 2008, *PASP*, **120**, 1233
- Jakobsen, P., Ferruit, P., Alves de Oliveira, C., et al. 2022, *A&A*, **661**, A80
- Jarrett, T. H., Cohen, M., Masci, F., et al. 2011, *ApJ*, **735**, 112
- Kimble, R. A., MacKenty, J. W., O'Connell, R. W., & Townsend, J. A. 2008, *Proc. SPIE*, **7010**, 43
- Kirkpatrick, J. D., Cushing, M. C., Gelino, C. R., et al. 2011, *ApJS*, **197**, 19
- Kirkpatrick, J. D., Cushing, M. C., Gelino, C. R., et al. 2013, *ApJ*, **776**, 128
- Kirkpatrick, J. D., Gelino, C. R., Cushing, M. C., et al. 2012, *ApJ*, **753**, 156
- Kirkpatrick, J. D., Gelino, C. R., Faherty, J. K., et al. 2021, *ApJS*, **253**, 7
- Kirkpatrick, J. D., Martin, E. C., Smart, R. L., et al. 2019, *ApJS*, **240**, 19
- Kirkpatrick, J. D., Schneider, A., Fajardo-Acosta, S., et al. 2014, *ApJ*, **783**, 122
- Kopytova, T. G., Crossfield, I. J. M., Deacon, N. R., et al. 2014, *ApJ*, **797**, 3
- Krick, J. E., Lowrance, P., Carey, S., et al. 2021, *AJ*, **161**, 177
- Lacy, B., & Burrows, A. 2023, *ApJ*, **950**, 8
- Leggett, S. K., Tremblin, P., Esplin, T. L., Luhman, K. L., & Morley, C. V. 2017, *ApJ*, **842**, 118
- Leggett, S. K., Tremblin, P., Phillips, M. W., et al. 2021, *ApJ*, **918**, 11
- Line, M. R., Marley, M. S., Liu, M. C., et al. 2017, *ApJ*, **848**, 83
- Liu, M. C., Deacon, N. R., Magnier, E. A., et al. 2011, *ApJL*, **740**, L32
- Liu, M. C., Dupuy, T. J., Bowler, B. P., Leggett, S. K., & Best, W. M. J. 2012, *ApJ*, **758**, 57
- Luhman, K. L. 2014a, *ApJ*, **781**, 4
- Luhman, K. L. 2014b, *ApJL*, **786**, L18
- Luhman, K. L., Burgasser, A. J., & Bochanski, J. J. 2011, *ApJL*, **730**, L9
- Luhman, K. L., Burgasser, A. J., Labbé, I., et al. 2012, *ApJ*, **744**, 135
- Luhman, K. L., & Esplin, T. L. 2014, *ApJ*, **796**, 6
- Luhman, K. L., & Esplin, T. L. 2016, *AJ*, **152**, 78
- Mainzer, A., Bauer, J., Cutri, R. M., et al. 2014, *ApJ*, **792**, 30
- Mang, J., Gao, P., Hood, C. E., et al. 2022, *ApJ*, **927**, 184
- Marley, M. S., Saumon, D., Visscher, C., et al. 2021, *ApJ*, **920**, 85
- Marocco, F., Caselden, D., Meisner, A. M., et al. 2019, *ApJ*, **881**, 17
- Marocco, F., Kirkpatrick, J. D., Meisner, A. M., et al. 2020, *ApJL*, **888**, L19
- Meisner, A. M., Caselden, D., Kirkpatrick, J. D., et al. 2020a, *ApJ*, **889**, 74
- Meisner, A. M., Faherty, J. K., Kirkpatrick, J. D., et al. 2020b, *ApJ*, **899**, 123
- Meisner, A. M., Leggett, S. K., Logsdon, S. E., et al. 2023, *AJ*, **166**, 57
- Miles, B. E., Skemer, A. J. I., Morley, C. V., et al. 2020, *AJ*, **160**, 63
- Morley, C. V., Fortney, J. J., Marley, M. S., et al. 2012, *ApJ*, **756**, 172
- Morley, C. V., Marley, M. S., Fortney, J. J., & Lupu, R. 2014a, *ApJL*, **789**, L14
- Morley, C. V., Marley, M. S., Fortney, J. J., et al. 2014b, *ApJ*, **787**, 78
- Morley, C. V., Skemer, A. J., Allers, K. N., et al. 2018, *ApJ*, **858**, 97
- Mukherjee, S., Fortney, J. J., Batalha, N. E., et al. 2022, *ApJ*, **938**, 107
- Phillips, M. W., Tremblin, P., Baraffe, I., et al. 2020, *A&A*, **637**, A38
- Pinfield, D. J., Gromadzki, M., Leggett, S. K., et al. 2014, *MNRAS*, **444**, 1931
- Prinn, R. G., & Lewis, J. S. 1975, *Sci*, **190**, 274
- Rieke, G. H., Engelke, C., Su, K., & Casagrande, L. 2023, *AJ*, **165**, 99
- Rieke, G. H., Wright, G. S., Böker, T., et al. 2015, *PASP*, **127**, 584
- Robbins, G., Meisner, A. M., Schneider, A. C., et al. 2023, *ApJ*, **958**, 94
- Rowland, M. J., Morley, C. V., & Line, M. R. 2023, *ApJ*, **947**, 6
- Saumon, D., & Marley, M. S. 2008, *ApJ*, **689**, 1327
- Saumon, D., Marley, M. S., Abel, M., Frommhold, L., & Freedman, R. S. 2012, *ApJ*, **750**, 74
- Schneider, A. C., Cushing, M. C., Kirkpatrick, J. D., & Gelino, C. R. 2016, *ApJL*, **823**, L35
- Schneider, A. C., Cushing, M. C., Kirkpatrick, J. D., et al. 2015, *ApJ*, **804**, 92
- Schneider, A. C., Meisner, A. M., Gagné, J., et al. 2021, *ApJ*, **921**, 140
- Skemer, A. J., Morley, C. V., Allers, K. N., et al. 2016, *ApJL*, **826**, L17
- Tang, S.-Y., Robinson, T. D., Marley, M. S., et al. 2021, *ApJ*, **922**, 26
- Tinney, C. G., Faherty, J. K., Kirkpatrick, J. D., et al. 2012, *ApJ*, **759**, 60
- Tinney, C. G., Kirkpatrick, J. D., Faherty, J. K., et al. 2018, *ApJS*, **236**, 28
- Tremblin, P., Amundsen, D. S., Mourier, P., et al. 2015, *ApJL*, **804**, L17
- Visscher, C., Lodders, K., & Fegley, B., Jr. 2006, *ApJ*, **648**, 1181
- Werner, M. W., Roellig, T. L., Low, F. J., et al. 2004, *ApJS*, **154**, 1
- Wright, E. L., Eisenhardt, P. R. M., Mainzer, A. K., et al. 2010, *AJ*, **140**, 1868
- Wright, E. L., Mainzer, A., Kirkpatrick, J. D., et al. 2014, *AJ*, **148**, 82
- Zalesky, J. A., Line, M. R., Schneider, A. C., & Patience, J. 2019, *ApJ*, **877**, 24
- Zapatero Osorio, M. R., Lodieu, N., Béjar, V. J. S., et al. 2016, *A&A*, **592**, A80